

Investigation of the effects of domain representation and boundary condition selection in numerical simulations of micro scale flows with phase change

Daniel Pearce^{*1}, Konstantina Vogiatzaki², A.M.K.P Taylor³, Y. Hardalupas³

¹Delphi Diesel Systems Ltd, Imperial College, London, UK

²Advanced Engineering Center, University of Brighton, UK

³Mechanical Engineering Department, Imperial College, London, UK

*Corresponding author: Daniel.Pearce@delphi.com

Abstract

Cavitation is a research area of high industrial interest due to the significant role it plays in the droplet formation and spray breakup in various processes such as flows in micro channels, microsensors and fuel injectors. In the current work we explore the predictive capabilities of a numerical framework within Large Eddy Simulation context when Diesel is used as working fluid and is injected at various pressures through a micro-channel. Results in terms of void fraction, velocity and pressure are compared with the experimental data of Winklhofer [30,31]. Our focus is cavitation within the channel as well as in the downstream jet. Moreover, since cavitation is a phenomenon affected considerably by the underlying pressure waves that occur on similar time and length scales as the bubble dynamics, the sensitivity of the predictions to the downstream domain and boundary representation will be addressed.

Keywords

cavitation, LES, pressure waves, OpenFOAM

Introduction

The term cavitation is used to describe the phenomenon of vapour production within a homogeneous liquid due to the pressure reduction below the vapour pressure of the liquid. This may be achieved in static situations by, for example, lowering the atmospheric pressure acting on the surface of a liquid (which resembles boiling but does not require a temperature change) but may also occur dynamically. Dynamically occurring cavitation is when the local flow conditions are such that the fluid can no longer follow the geometry, it detaches and low pressure regions are caused on the surface as in propellers, hydrofoils etc. In orifices and nozzles the high speed flow through the throat causes low pressure along with eddies and recirculation zones in which cavitation is generated. In a final example of dynamically occurring cavitation, the turbulent shear layer of craya-curtet jets may be strong enough to generate vortices in which the local pressure at the vortex core is below the vapour pressure and hence cavitation may be produced [3]. A more comprehensive review of the various forms of cavitation may be found in Franc [12], Bergant [4], Dumont [7] and Arndt [2, 3].

In the present study, we examine cavitation as it occurs within micro channels, often used as a simplified approximation for a nozzle. Nozzles are fundamental to a wide range of industrial processes such as spray painting, jet cutting and fuel injection systems. This application was chosen for a number of reasons: the geometry is simple but can be exactly matched to experimental evidence such as Winklhofer et al [31] or Mauger et al [18], the problem is of commercial interest (e.g. to support emissions regulations) and there exists a wide body of previous studies upon which to build. The specific difficulties around the conditions found in typical injection systems may also be seen as an extreme case with which a numerical modelling scheme would need to cope with. This extends the work to have a wider field of application to the general problem of numerical simulation of hydrodynamic cavitating flows.

In this paper we assess the predictive capabilities of a numerical framework within the Large Eddy Simulation context when Diesel fuel is injected at various pressures through a micro-channel. In particular, the aim was to improve model behaviour in the range of critical cavitation and beyond. Critical cavitation is defined as the point at which the flow ceases to be pressure dependent and has reached a maxima for mass flow (known as 'choked' conditions). If the pressure difference is greater than that required for choked conditions, the cavitation region may cover the full spanwise extent of the channel and be 'fully choked'. This area between choked and fully choked is poorly reproduced by simulation currently in the literature. In order to correctly capture the real conditions within the nozzle, the nozzle exit pressure is of primary importance and for this to be accurate, the downstream domain must contain the relevant features that effect this pressure. Thus, the downstream length and boundary condition were varied parametrically. The second feature of importance is the presence of pressure waves in domain which can substantially change the transient nozzle exit pressure. For these reasons, the experimental data at a measured downstream pressure value were compared to different pressure values of both fixed and wave transmitting domain terminations in order to attempt to replicate the correct pressure at the nozzle exit.

The structure is as follows: We first present our numerical framework as well as the experimental set up. We explain in detail the important sub models used (phase change, turbulence and compressibility) as well as the numerical parameters that affect the results (physical properties, grid and boundary conditions). A sensitivity analysis for all the aforementioned models and parameters is not possible here due to space limitations. Thus, in the result section we chose to present the sensitivity of the predictions to the selection of pressure boundary conditions that are not well represented in the literature up to date. We present the numerical results in terms of void fraction, velocity and pressure and we compare them with the corresponding experimental data [31].

Experimental Setup

The simulations in this work are compared to experiments performed by AVL. The setup is described in [31] and the model nozzle is shown in Fig. 1. Diesel fuel is pumped through a micro channel eroded into a 0.3 mm thick steel sheet which is sandwiched between two sapphire windows, allowing the visualisation of the channel and forming a nozzle-like structure. The geometry analysed here corresponds to the throttle geometry called "U" in [31], which is a rectangular shaped channel of 100 x 301 x 284 mm with an inlet radius of 20 μm. The channel extends 10 mm before and after the nozzle to minimise the effect of the boundary conditions within the nozzle. In all of the experimental cases the upstream pressure is 100 bar, and the outlet pressure is varied. The three outlet pressures used here for comparison are 50 bar, 30 bar and 15 bar in order to also allow for comparison with results presented in the work of [5, 14, 25].

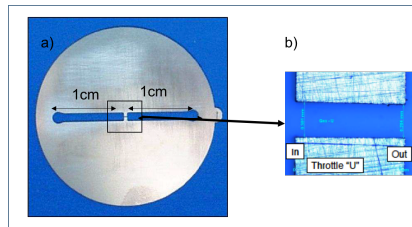


Figure 1. (a) View of the experimental nozzle (b) Zoom-in in throttle geometry U. [31]

Numerical Parameters

In this work, OpenFOAM [11] was chosen as the code base due to its extensible nature with access to the source code, in order to create and modify the governing numerics. A brief description of the governing equations, phase change, turbulence and compressibility sub models as well as grid specifics are presented in the following section. Special focus is given to the choice of the boundary conditions that is the main topic of this work.

Multiphase modelling including compressibility

For the simulation of the two phases present (gas and liquid) in the domain we are using the so called "one-fluid approach" within a compressible framework. Instead of having an individual set of transport equations for each phase, in every computational cell liquid and vapour are treated as one continuum. The compressibilities of both phases are taken into account and the temperature is assumed to be constant. The one fluid approach is suitable for problems where the second phase may be considered to be fully dispersed within the first such as 'cloud cavitation' or strongly turbulent cavitation of numerous small, discrete bubbles. It is less well suited to slug flow or stratified flow situations where the two phases might reasonably be expected to have differing velocities. In our case and given the high pressure differences for the geometry under consideration, this approach can be considered as a reasonable assumption.

The starting point of forming the numerical framework used is the following equation of continuity

$$\frac{D\bar{\rho}}{Dt} = \psi \frac{D\bar{\rho}}{Dt} \quad (1)$$

which is based on a barotropic equation of state. The term ψ is the compressibility of the mixture which is defined as $\psi = 1/c^2$ and needs to be determined. Equation 1 can either be used directly in the continuity equation to formulate a pressure equation, or integrated to obtain the pressure as a function of the density as suggested by Schmidt et al [26]. In our case we use the former approach following [14]. We use the notation with bars over the quantities since the framework is formulated within the LES context. The equation of state for the mixture should then be consistent with the liquid and the vapour equations of state, both at the limits when there is pure liquid or pure vapour, and also at the intermediate states when there is a mixture. The densities of the two phases are defined as:

$$\bar{\rho}_v = \psi_v \bar{\rho} \quad (2)$$

$$\bar{\rho}_l = \bar{\rho}_l^0 + \psi_l \bar{p} \quad (3)$$

The terms ψ_v and ψ_l are the compressibility factors of vapour and liquid respectively. In order to separate the amount of volume that each phase occupies in this "mixture" fluid a phase indicator function known as the vapour fraction, α , is used. α is defined as

$$\bar{\alpha} = \frac{\bar{p} - \bar{\rho}_{l,sat}}{\bar{\rho}_{v,sat} - \bar{\rho}_{l,sat}} \quad (4)$$

where

$$\bar{\rho}_{v,sat} = \psi_v \bar{p}_{sat} \quad (5)$$

It can be seen that if there is no cavitation within a cell then $\bar{p} = \bar{p}_{l,sat}$ resulting in $\alpha = 0$ while for the case that a cell is full of vapour $\bar{p} = \bar{p}_{v,sat}$ and $\alpha = 1$. The equilibrium model as described above has as its main advantage its simplicity. There is no need to solve an additional transport equation for the vapour volume fraction, since the fluid above the vapour pressure is defined as a liquid, the fluid below the vapour pressure as vapour and the change of density with pressure is defined by an equation of state. Moreover, since it is based on local equilibrium assumption it ignores the effect of the interfacial forces between different phases and thus the surface tension term in the momentum equation is considered negligible. Models of this category are more appropriate for high speed nozzle flows in that the effect of surface tension is minimised resulting in an homogeneous mixture of bubbles and liquid in each cell such as in diesel fuel injectors [8]. The model has been compared with alternative models accounting for interfacial forces in our previous work [27] for various cavitation numbers but for a larger scale geometry (lower velocity) and results indicated a similar behaviour of the two models as the cavitation number was increasing. Combining Eqs. 2,3,4 we form the mixture's equilibrium equation of state.

$$\bar{p} = (1 - \alpha) \bar{p}_l^0 + [\alpha \psi_v + (1 - \alpha) \psi_l] p_{sat} + \psi(p - p_{sat}) \quad (6)$$

The equations of motion are then closed with the constitutive relations for the density ρ , the dynamic viscosity, μ and the compressibility ψ :

$$\mu = \alpha \mu_v + (1 - \alpha) \mu_l \quad (7)$$

$$\bar{p} = (1 - \alpha) \bar{p}_l^0 + [\alpha \psi_v + (1 - \alpha) \psi_l] p_{sat} + \psi(p - p_{sat}) \quad (8)$$

$$\bar{\psi} = \alpha \bar{\psi}_v + (1 - \alpha) \bar{\psi}_l \quad (9)$$

Compressibility and Thermophysical properties

A linear model for compressibility was used since it is considered more consistent with the VOF-method, where viscosity and mass fraction are similarly described by linear equations [14].

$$\bar{\psi} = \alpha \bar{\psi}_v + (1 - \alpha) \bar{\psi}_l \quad (10)$$

When Eq.10 is used then the equation of state for the liquid can be reduced to a linear equation as well with $\bar{p}_{l,vap} = \rho_{l,sat} + \psi_p$. Alternative models are the Chung [6] and the Wallis model [28]. Literature [13] suggests that the Wallis model represents the lower speed of sound (compressibility) in a bubbly mixture in a more physical way, but it is rather unstable when used for high speed flows.

In terms of the choice of the individual compressibility factors ψ_l and ψ_v the physical properties of the diesel fuel have to be considered. The difficulty in the use of Diesel in numerical simulations is that as a fuel it typically varies seasonally as well as geographically so its properties are generally defined in terms of a range rather than a specific value. For example in Europe, the specification of common pump diesel must conform to EN590 [1] (which is more concerned with sulfur content and biofuel components due to their effect on emissions) so that the stated density must be between 820 and 845 kg/m^3 . Koukouvinis et al [15] chose to use a value well outside this range in order to help tune their model and reduce the propensity of the code to develop significant negative pressures. Habchi et al [9] also chose a value outside the EN590 range from some of their earlier work on lumped parameter modelling [10] which was focused on vaporisation rates and simulating spray conditions at 400K. The selection of subcomponents and use of a gas derived EOS may explain this lower than usual density value. All other authors reviewed chose values close to the EN590 range but it is generally unclear if this is for convenience or it served to help drive model outputs. For the current simulations the following (see Table 1) thermodynamic properties have been adopted.

Turbulence and the Sub - Grid scales

Turbulence in the context of small scale , high speed flow is difficult to interpret within the realm of multiphase flows since not only are the mechanisms poorly understood [23] but the transition to fully developed turbulent flow which might be expected as the Reynolds number increases can be delayed significantly. Established vapour regions near the wall can reduce the effective viscosity and associated frictional losses such that the central jet can persist in a turbulent transition regime for wide range of pressure differentials. In this study therefore, a transient methodology is required (LES) even though the problem is quasi-steady state. It should be noticed that one of the difficulties in performing LES in the context of cavitation is that it is hard to determine the length scale spectrum and the resolution requirements. Although in single phase flows the smallest scale is defined through the Kolmogorov scale, in two phase flows the definitions of an equivalent scale is difficult. In the current work we model the sub-grid tensor term with an algebraic eddy viscosity models in which the stress tensor τ_{ij}^{sgs} is related to the resolved strain rate tensor \tilde{S}_{ij} by means of a scalar eddy viscosity given by an algebraic equation. It is based on the Boussinesq hypothesis associating τ_{ij}^{sgs} with a sgs turbulent viscosity μ_T . The idea is that the momentum transfer caused by turbulent eddies can be modelled with an eddy viscosity in the same way the momentum transfer caused by the molecular motion in a gas can be described by a molecular viscosity. The model is known as the Wall-Adapting Local Eddy-viscosity model (WALE) [19]. The sgs viscosity is dynamically computed with the square of the velocity gradient tensor rather than the resolved strain rate used in Smagorinsky-type models. This velocity tensor can not only account for the effects of both strain and rotation rate of the smallest resolved turbulence fluctuations, but also recovers the proper near-wall scaling for the eddy viscosity without requiring dynamic procedures. Moreover, as the WALE model is invariant to any coordinate translation or rotation and no test-filtering operation is needed, it is therefore well suited for LES in complex geometries [19].

Boundary conditions

In the course of reviewing existent literature on simulation of cavitating channels it was found that there exists a dearth of information on the downstream length requirements in order to correctly satisfy a pressure governed boundary condition. In Winklhofer's experiment fuel pressure levels are measured 35 mm upstream and downstream of the observation element. This will be referred for the rest of the paper as " P_{out} " while the pressure used in the numerical simulations as " $P_{boundary}$ ". These two pressures do not necessarily coincide even if the same case is under consideration since " $P_{boundary}$ " is dependent on the size of the simulated geometry that imposes a specific pressure drop in between the exit of the nozzle and the experimentally measured boundary condition of the domain. It may also allow different levels of pressure wave reflection. It should also be noted that in the experiment, the gauge used may be damped in order to observe a smooth value for monitoring purposes. Even with a high fidelity pressure sensor, the reported values have lost the richness of the full signal content which would have been an indicator of the frequency and amplitude of any transient fluctuations. " P_{out} " should then be considered to be time averaged with a possibly unknown fluctuating component. In most models the downstream distance to the outlet boundary is severely truncated in the name of reducing overall cell count and calculation time. Examples of zero downstream length include [29], [20] and [17] while those classified as 'short' -between 1-5 diameters include [15] while [22] utilise larger exit domains with extra geometrical features. In this study, we consider the effects of the downstream length by varying the distance from the outlet of the channel section to the boundary by 5, 9 and 12mm (keeping in mind that the channel length is 1mm while the length of the geometry before the nozzle is also simulated as 1 mm). Thus, the 12mm long case essentially represents the size of the experimental geometry closely. One additional case with 3mm length was tested however it is not represented here since the close proximity of the exit boundary to the nozzle outlet led to considerable numerical instabilities.

The boundary conditions were treated as a total pressure condition at the inlet to the domain with a small component of turbulent kinetic energy and negligible velocity. For the the outlet boundary condition, two variations were tested. The first configuration is typical for this type of problem and uses a fixed value condition (FP) imposed as a pressure constraint to ensure that the equations are well bounded. This type of problem is the classic 'pressure driven flow' scenario in which the velocity at the domain exit is considered to be a dependant variable. The second configuration tested was a novel variant of the pressure wave transmissive (PWT) condition that was modified to be compatible for multiphase problems. The PWT condition attempts to transmit all incident pressure waves outside the domain and maintain a given far field value of pressure. This is done by attempting to keep the instantaneous value 'close' to the given far field value. In this sense 'close' is defined by a separate parameter, the far field distance. A smaller far field distance implies that a smaller deviation is allowed from its prescribed value whilst a larger far field distance allows greater deviation. The core scheme for this is derived from Poinot [21] and is accomplishing by assuming that for high Reynolds flows, the hyperbolic part of the Navier Stokes equations represent the wave component of the local pressure field.

Table 1. Thermodynamic properties of Diesel

$p_{sat} (Pa)$	$\rho_{l,sat} (kg/m^3)$	$\rho_{v,sat} (kg/m^3)$	ψ_l	ψ_v
5400	832	0.1361	0.0000005	0.0000025

Grid

The cell size in nozzle that is the area of interest is 0.02mm while outside the nozzle is 0.06mm . The Reynolds numbers considered for all three outlet pressure cases (15bar, 30bar, 50bar) is of the order of 10^6 while the Taylor scale is of the order of 0.001mm . The total number of cells was varied depending the size of the geometry in order to maintain a constant resolution. The near wall region was resolved to typical values of y^+ of the order 1-5 such that the LES terms are considered to be implicit. To ensure a stable solution, transient calculations of $250\ \mu\text{s}$ were performed. The convergence criteria used for the calculations are based on the values of the residuals (which have to reach a value of 10^{-7} at least for all equations) and the mass flow rate (which has to be stabilized as much as possible). The time step is limited by both the Courant number (taken as 0.2) and the acoustic Courant number (taken as 12).

Results

Figure 2 shows the vapour fraction, pressure and velocity instantaneous fields for the 5mm domain geometry at time $t=0.075\text{ms}$ using FP boundary conditions. Three different outlet pressure values are presented. Looking at the α profiles it can be seen that as the outlet pressure is increased the amount of vapour within the nozzle reduces and this is comparable with the experimental observations [31]. Also, although a structure resembling a cavitation cloud is evident after the nozzle exit for $P_{\text{boundary}} = 15\text{bar}$ this disappears for higher pressures. Looking at the velocity and pressure plots (especially at the area outside the nozzle) it can be seen that using a FP boundary condition leads to 'pulses' in the jet velocity with alternating fast and slow regions with similar vector directions, implying that the rotation is low and there is no significant reverse flow. This oscillation of the velocity magnitude has several implications to the overall flow structures that may be observed. We suggest that these velocity fluctuations are a result of the pressure waves trapped in the domain reflecting and interacting at nodal points so local high and low pressure regions act to retard or accelerate the jet as it moves away from the nozzle. The challenge that arises in numerical simulations using FP boundary conditions is that there is not a straight forward way to separate pressure waves associated with the pressure outlet conditions and pressure waves that occur naturally because of the nozzle operating conditions. By considering a PWT boundary condition as we suggest in this work we have the potential to better control of the waves that are allowed to reflect within the domain and thus help us separate which phenomena are associated with naturally occurring waves and which ones are related to numerical artefacts

One implication relevant to pressure prediction that is evident from the plots of Fig. 2 is that local pressure differences in streamwise sections of the downstream domain drive velocity profile differences in the shear layer which in turn effect local low pressure regions in which cavitation is likely. It is interesting to note that an examination of the vorticity associated with this flow shows very little correlation and no clear vortical structures could be observed. The pressure and velocity plots in Fig. 2 have additional black contours added to highlight those areas where the pressure is less than the vapour pressure. Cavitation is not observed for the 55bar outlet pressure case and only observed in the region of the vena contracta for the 30bar case. The 30bar velocity plot shows how the jet shear layer undergoes velocity differences along the jet centreline while the 15bar velocity plot shows how greater differentials can lead to vapour formation in the shear layer. It is evident that correct prediction of the pressure waves in the domain is an important factor in the overall solution.

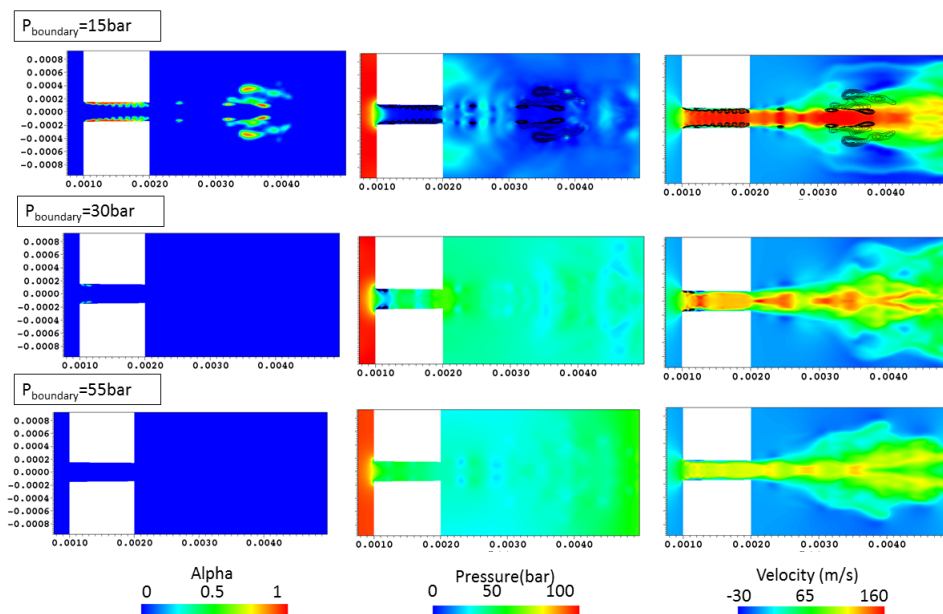


Figure 2. Instantaneous contour plots of vapour fraction, pressure and axial velocity at $t=.075\text{s}$. Boundary condition is considered as fixed pressure. Axis scale is m .

Another implication is that the variable pressure difference across the nozzle due to these wave effects can lead

to instabilities in the cavitation which is generated in the usual vena contracta regions and along the nozzle walls. Supercavitation is partially suppressed and the vapour along the nozzle walls may not always extend fully to the exit with small backflow into the channel as the local pressure at the exit corner is higher than the vapour pressure. The momentum of the jet inside the nozzle is high enough that the boundary between the fast moving fluid and the near static vapour is essentially fixed after the initial jet acceleration.

An additional important remark from these plots is relevant to the cavitation evolution in the nozzle for the 30bar exit pressure that is identified in the experiments as the critical cavitation case (see Fig 3). The experimental data indicates that cavitation and the subsequent 'bubbly' mixture could extend the entire spanwise section of the channel as critical cavitation pressure differentials are exceeded. For the U geometry, this evolution occurs rapidly after the exit pressure is reduced below 30bar, as even 29bar exit pressure has substantially increased cavitation probability. This could explain why that the simulated 30bar FP case (seen in Fig. 2) which is particularly close to a high sensitivity region shows a low cavitation region within the nozzle.

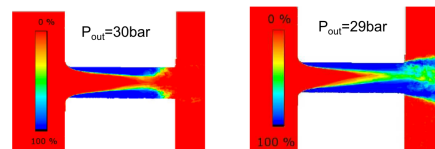


Figure 3. Experimental cavitation probability at critical cavitation point and beyond [31].

In order to better understand the effect of pressure waves within the domain, the wave transmissive boundary condition is applied at the outlet. This configuration was tested at 20bar far field pressure with 5, 9 and 18mm far field distance values. Although with this approach waves are able to exit the domain as expected, (in theory limiting the effect of artificial pressure oscillations) some pressure variations are still present because of the high Re number of the flow. These instabilities interact with the vapour fraction leading to vapour collapse events in the downstream area. These collapse events trigger pressure waves which are then able to travel upstream towards the nozzle in a similar way as that which occurs in the experiment. We first zoom into the nozzle cavitation development for the 15bar FP case and 20bar PWT (see Fig. 4). The experimental evidence [31] is that under these conditions the cavitation should extend to the nozzle centreline leading to fully choked conditions. In our simulations we can also see some indication of the cavitation regions beginning to close on the centreline for the FB conditions, something that is largely missing from other simulations of similar geometries. In contrast it can be noted that as the pressure waves are allowed to escape the domain, the cavitation in the PWT case lacks turbulent features and more closely resembles lower pressure cases. This highlights the impact that reflections from the boundary (either physical or artificial) have on the nozzle cavitation regime. Previous work such as [16] and [24] for example have examined the same geometry but have not addressed this issue, i.e. that fully choked flow conditions are met. In contrast in Fig. 4 we can see that when waves are allowed to travel back to the domain then the framework is capable of representing some of the important features. Of course further understanding is needed since the waves in the case of FP are more relevant to the length of the domain rather than the actual present in the domain because of the injection conditions. In previous work of [14], in order to increase the amount of vapour within the nozzle the upper and lower walls were considered with a slip condition for the velocity, similar to that used in supersonic compressible flow. This was done under the assumption that a no-slip boundary condition would lead to overestimates of the thickness of the boundary layer, resulting in strong vortices in the centre of the channel and incorrect modelling of the flow's cavitation. The assumption of a slip condition seems rather unphysical and according to our observations a re-examination of the boundary conditions might be more beneficial.

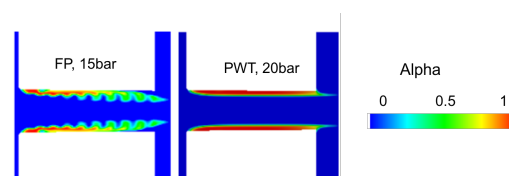


Figure 4. Vapour fraction in nozzle region, Left: 15bar FP, 5mm downstream length. Right 20bar PWT, far field 5mm

Figure 5 shows a comparison of the pressure profiles along the centreline of the nozzle for a selection of the tested configurations. The experimental profile inside the nozzle is characterised by an initial pressure drop because of the flow turn at the inlet as well as a sudden pressure rise at around 0.5mm downstream. It can be seen that for the 15bar cases that FP conditions are used only the case of 5mm captures the correct behaviour. This does not necessarily mean that this boundary condition is accurate. It only indicates that since we have set the boundary 5mm downstream the exit of the nozzle and this specific boundary imposes reflection of pressure waves these waves travelled back upstream inside the nozzle recovering some of the behaviour present in experiments. For the other two cases (9mm and 12mm) that in reality are closer to the real experimental geometry, the pressure drop is over-predicted inside the nozzle. The pressure only partially recovers because of the pressure increase at the

exit. Results are similar to previous studies in the literature [13]. Looking at the poor agreement of the prediction of the 9mm and the 12mm case even after the nozzle exit (at 1.5mm) one can argue that since we impose 15bar pressure at 9mm and 12mm boundary we cannot really predict accurately the pressure difference measured by the experiment at 35mm downstream of the nozzle. In an effort to better tune our results we include the results of a 9mm geometry with $P_{boundary}=20bar$. We can see that with this re-adjustment although the results match better at 1.5mm, the predictions inside the nozzle are still poor. Changing the boundary to wave transmissive conditions gives two important advantages. One is that for both 5mm far field and 18mm far field values, part of the correct in nozzle pressure profile is recovered. Moreover, with this method the size of the simulated geometry is not changed (this is always 5mm), instead the far field parameter is controlled and hence the amount of waves allowed within the domain. This considerably reduces the computational cost in comparison to FP conditions in which the geometry was varied in order to control the boundary response.

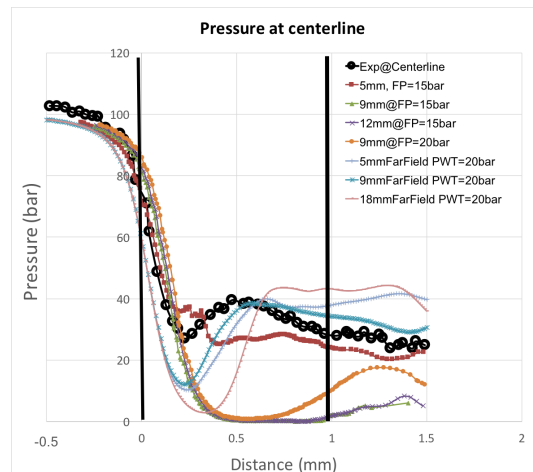


Figure 5. Pressure profiles along nozzle centreline comparing experimental data at 30bar to various downstream pressure values

Figure 6 shows the spanwise velocity profiles for the 15bar experimental condition at $x=0.17mm$. Five numerical cases are considered (three with FP boundaries and two with PWT). The experimental data shows a peak in velocity towards the nozzle upper and lower boundaries which is indicative of the lower viscosity and hence frictional losses in this area because of cavitation. It also shows a recovery of the velocity in the nozzle core although it does not achieve a maxima. The 15bar, 5mm downstream FP case is best able to reproduce this result although it does not show the higher central area. The PWT condition shows a flatter profile which indicates that the shape of the FP conditions is being influenced by wave reflections present in the downstream area. The wave transmissive cases also demonstrate the differences seen across the various far field values that were used. Figure 6 has far field values of 5mm and 9mm, all at the same $P_{boundary}$ of 20bar. A linear trend in the maximum velocity as the far field values increase can be seen. Note that the 9mm case with FP and the 9mm PWT both at 20 bar predict similar velocity magnitude at the centerline but they differ in the prediction at the layer closer to the wall. This can be considered as an indication that capturing the pressure waves better within the domain is not expected to change considerably the main jet behaviour but it is expected to change the cavitation predictions. Further variations of the wave transmissive case are currently running in order to better explore this relationship although they were not available at the time of writing.

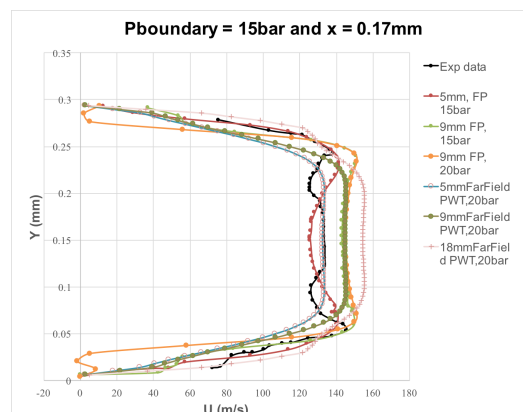


Figure 6. Spanwise Velocity plots at $x=.17mm$ comparing experimental data at 15bar to various downstream pressure values

Conclusions

The downstream boundary conditions of a micro-channel geometry with in nozzle cavitation at critical cavitation and fully choked flow conditions were examined and their impact assessed. The domain bounds and definition have been shown to be an area poorly understood with regards to their effect on in nozzle results. Using rigid exit conditions mean that pressure waves generated within the nozzle or the downstream domain are reflected and continue to influence the local flow conditions. Downstream length and choice of boundary condition are therefore important in order to accurately model the pressure field and cavitation within the nozzle. The outlet from the nozzle section is prone to external cavitation in the shear layer (for choked flow conditions) which can also impact the nozzle exit pressure, particularly when attempting to validate against experimental results where the downstream pressure may be measured at a location some distance from the nozzle itself. It was found that vorticity (especially for cavitation developed outside the nozzle) did not play a large part in external cavitation formation, rather the velocity difference in the shear zone interacting with pressure waves had the greatest influence. A novel wave transmissive boundary condition for multiphase flow was tested and shown to be promising in replicating in nozzle pressure profiles compared to more traditional fixed boundary conditions. However it was proven less accurate in replicating the velocity profile close to the wall. Further work needs to be done in order to confirm the stability of the wave transmissive boundary with regards to vapour formation in the far field.

References

- [1] Anon. BS EN590:2013, 2013.
- [2] R. Arndt. *Annual Review of Fluid Mechanics*, pages 273–328, 1981.
- [3] R. Arndt. *Annual Review of Fluid Mechanics*, (34):143–175, 2002.
- [4] A. Bergant, R. Simpson, and S. Tijsseling. *Journal of Fluids and Structures*, 22(2):135–171, feb 2006.
- [5] Federico Brusiani, Sergio Negro, Gian Marco Bianchi, Maryam Moulai, Kshitij Neroorkar, and David Schmidt. *SAE paper 2013-01-1613*, 2013.
- [6] M. S. Chung, S. B. Park, and H. K. Lee. *Journal of Sound and Vibration*, 276(1-2):13–26, 2004.
- [7] N. Dumont, O. Simonin, and C. Habchi. *8th International conference on Liquid Atomisation and Spray systems*, 2000.
- [8] C.P. Egerer, S. Hickel, S. J. Schmidt, and N. Adams. *Physics of Fluids*, 26(8), 2014.
- [9] C. Habchi, N. Dumont, and O. Simonin. *Atomization and Sprays*, 18(2):129–162, 2008.
- [10] C Habchi, FA Lafossas, P Beard, and D Broseta. *SAE paper 2004-01-1996*, 2004.
- [11] C.W Hirt and B.D Nichols. *Journal of Computational Physics*, 39(1):201 – 225, 1981.
- [12] Jean-Pierre Franc and Jean-Marie Michel. *Fundamentals of Cavitation*. Kluwer Academic Publishers, Dordrecht, 2004.
- [13] F.P. Kärrholm. *Numerical modelling of diesel spray injection, turbulence interaction and combustion*. PhD thesis, Goteborg, 2008.
- [14] F.P. Kärrholm, H. Weller, and N. Nordin. *5th Joint ASME/JSME Fluids Engineering Conference*, pages 465–474, 2007.
- [15] P. Koukouvinis, M. Gavaises, J. Li, and L. Wang. *Journal of Physics: Conference Series 9th International Symposium on Cavitation*, 656:012088, 2015.
- [16] X. Margot, S. Hoyas, A. Gil, and S. Patouna. *Engineering Applications of Computational Fluid Mechanics*, 6(1):15–24, 2012.
- [17] Sergey Martynov. *Analysis*, (September):1–226, 2005.
- [18] Cyril Mauger, Loïc Méès, Marc Michard, Alexandre Azouzi, and Stéphane Valette. *Experiments in Fluids*, 53(6):1895–1913, 2012.
- [19] F. Nicoud and F. Ducros. *Flow, Turbulence and Combustion*, 62(3):183–200, 1999.
- [20] Stavroula Patouna. *A CFD STUDY OF CAVITATION IN REAL SIZE DIESEL INJECTORS*. PhD thesis, University Polytechnica Valencia, 2012.
- [21] T.J. Poinsot and S.K. Lele. *Journal of Computational Physics*, 99(2):352, apr 1992.
- [22] Tao Qiu, Xin Song, Yan Lei, Xinghua Liu, Xiaodong An, and Mingchia Lai. *Applied Thermal Engineering*, 109:364–372, 2016.
- [23] F. Ruiz and L. He. *Atomization and Sprays*, 9:419–429, 1999.
- [24] Kaushik Saha, Ehab Abu-Ramadan, and Xianguo Li. *Journal of Engineering for Gas Turbines and Power*, 135(6):062801, 2013.
- [25] F. J. Salvador, S. Hoyas, R. Novella, and J. Martinez-Lopez. *Proceedings of the Institution of Mechanical Engineers, Part D: Journal of Automobile Engineering*, 225(4):545–563, apr 2011.
- [26] David P. Schmidt, Christopher J. Rutland, and Michael L. Corradini. *Atomization and Sprays*, 9(3):255–276, 1999.
- [27] K. Vogiatzaki, P. Koukouvinis, and J. Carlton. *ILASS 2016*, (September):1–8, 2016.
- [28] G. B. Wallis. *One-dimensional two-phase flow*. McGraw-Hill, 1969.
- [29] Xiang Wang and WanHua Su. *Chinese Science Bulletin*, 54(10):1655–1662, may 2009.
- [30] E. Winklhofer, E. Kelz, and A. Morozov. *Proceedings of the ILASS-Europe Conference, Sorrento*, 2003.
- [31] E. Winklhofer, E. Kull, E. Kelz, and A. Morozov. *Proceedings of the ILASS-Europe Conference, Zurich*, 2001.